

Radiation Response of Group-IV and III-V Semiconductors Subjected to D-D and D-T Fusion Neutrons

Jean-Luc Autran, Daniela Munteanu

▶ **To cite this version:**

Jean-Luc Autran, Daniela Munteanu. Radiation Response of Group-IV and III-V Semiconductors Subjected to D-D and D-T Fusion Neutrons. New Advances in Semiconductors, IntechOpen, 2022, 10.5772/intechopen.103047 . hal-03695354

HAL Id: hal-03695354
https://amu.hal.science/hal-03695354

Submitted on 14 Jun 2022

HAL is a multi-disciplinary open access archive for the deposit and dissemination of scientific research documents, whether they are published or not. The documents may come from teaching and research institutions in France or abroad, or from public or private research centers.

L'archive ouverte pluridisciplinaire **HAL**, est destinée au dépôt et à la diffusion de documents scientifiques de niveau recherche, publiés ou non, émanant des établissements d'enseignement et de recherche français ou étrangers, des laboratoires publics ou privés.



Distributed under a Creative Commons Attribution| 4.0 International License

Chapter

Radiation Response of Group-IV and III-V Semiconductors Subjected to D–D and D–T Fusion Neutrons

Jean-Luc Autran and Daniela Munteanu

Abstract

This work focuses on the radiation response of Group IV (Si, Ge, SiC, diamond) and III-V (GaAs, GaN, GaP, GaSb, InAs, InP, InSb, AlAs) semiconductors subjected to D–D (2.45 MeV) and D–T (14 MeV) neutrons. The response of each material has been systematically investigated through a direct calculation using nuclear cross-section libraries, MCNP6, and Geant4 numerical simulations. For the semiconductor materials considered, we have investigated in detail the reaction rates per type of reaction (elastic, inelastic, and nonelastic) and proposed an exhaustive classification and counting of all the neutron-induced events and secondary products as a function of their nature and energy. Several metrics for quantifying the susceptibility of the related semiconductor-based electronics to neutron fusions have been finally considered and discussed.

Keywords: radiation effects, III-V compound semiconductors, fusion neutrons, D-D reaction, D-T reaction, numerical simulation, neutron cross section, elastic scattering, inelastic scattering, nonelastic interactions, nuclear data library, Geant4, MCNP, single-event effect

1. Introduction

At the horizon of 2035 and beyond, the very large electronic equipment for command and diagnostic operations of future fusion power machines, such as ITER, the international thermonuclear experimental reactor [1], will embrace a wide variety of semiconductors materials. Indeed, new materials, such as SiC, Ge, GaN, or GaAs, are envisaged to progressively replace the traditional silicon of microelectronics for high temperature, high performance, or high-speed electronics/optoelectronics applications [2–5]. These equipment will be directly or partially (behind radiation shielding) exposed to a complex radiation field due to primary fusion neutrons created in the core of the plasma and then transported outside the machine [6]. These neutrons are produced in the deuterium–tritium (D–T) reaction that has been identified as the most efficient for fusion devices [7]:

$$D + T \rightarrow {}^{4}He\ (3.52MeV) + n\ (14.07MeV) \quad (1)$$

However, one must also consider deuterium–deuterium (D–D) reaction because this less efficient fusion reaction will be used to study, during the development and commissioning of future machines, their operation before introducing tritium fuel. D–D fusion following the two main reactions with equal probability of occurrence:

$$D + D \rightarrow {}^{3}He\ (0.82MeV) + n(2.45MeV) \quad (2)$$

$$D + D \rightarrow T\ (1.01MeV) + p\ (3.02MeV) \quad (3)$$

For future fusion power machines, the radiative reliability issue for the envisaged new material-based electronics arises now, even if—(i) most of these components have not yet been manufactured and tested, and (ii) the design and the integration of machine electronics equipment will not take place for many years. In such a long-term development, numerical simulation offers a very promising solution to anticipate, in the first step at the material level, this reliability issue for semiconductors whose radiative response is little or poorly known.

In the direct continuation of our previous works [8–10] that investigated the atmospheric radiation response of a wide variety of semiconductors, the present chapter focuses on the radiation response of Group IV (Si, Ge, SiC, diamond) and III-V (GaAs, GaN, GaP, GaSb, InAs, InP, InSb, AlAs) semiconductors subjected to D–D (2.45 MeV) and D–T (14 MeV) neutrons.

In this work, the response of each material has been systematically investigated through a direct calculation using nuclear cross-section libraries, MCNP6, and Geant4 numerical simulations. In the following, for the 12 semiconductor materials considered, we will investigate in detail the reaction rates per type of reaction (elastic, inelastic, and nonelastic) and propose an exhaustive classification of all the neutron-induced secondary products as a function of their nature and distribution in the energy. Implications for quantifying the susceptibility of these related semiconductor-based electronics to neutron fusions will be finally presented and discussed.

2. Material properties

Table 1 summarizes the natural isotopic abundance of the different chemical elements entering the composition of the studied semiconductor materials. Nitrogen, phosphorus, and arsenic have only a single natural isotope which simplifies the calculations to come for these elements. On the contrary, the other elements have two (C, N, Ga, In, Sb), three (Si), and up to five (Ge) different natural isotopes. Nevertheless, for C and N, the relative weight of the minority isotope is less than or around the percent, so we can consider that the natural carbon and nitrogen consist only of the simple isotopes ^{12}C and ^{14}N, respectively, with a very good approximation. The other isotopes listed in **Table 1** must be considered with their respective weight in atomic composition for correctly simulating the neutron response of the natural materials to which they relate.

Table 2 reports the value of the energy bandgap, the number of atoms per square centimeter, the density, and the value of the energy for electron-hole pair creation in bulk material for the 12 semiconductors studied in this work. Due to their atomic composition and crystallographic structure, all these materials are denser than Si (2.33 g/cm^3) and three materials exhibit a much larger number of atoms per square centimeter than Si—SiC, diamond, and GaN. This can have a direct consequence on the

Symbol	Z	Nuclide (100×Z+A format)	Natural abundance (%)
C	6	6012	98.93
		6013	1.07
N	7	7014	99.6
		7015	0.4
Al	13	13027	100
		14028	92.22
Si	14	14029	4.68
		14030	3.09
P	15	15031	100
Ga	31	31069	60.1
		31071	39.9
		32070	20.52
		32072	27.45
Ge	32	32073	7.76
		32074	36.52
		32076	7.75
As	33	33075	100
In	49	49115	95.7
		49113	4.3
Sb	51	51121	57.4
		51123	42.6

Table 1.
Natural abundance of nuclides related to the materials studied in this work. Z refers to the atomic number, A to the atomic mass.

Material	Bandgap at 300 K (eV)	Number of atoms per cm^3 ($\times 10^{22}$)	Density (g/cm^3)	E-h pair creation energy Eeh (eV)
Si	1.124	5.0	2.329	3.6
Ge	0.661	4.42	5.3267	2.9
SiC (4H)	3.23	9.64	3.21	7.8
Diamond	5.47	17.6	3.515	12
GaAs	1.42	4.42	5.32	4.8
AlAs	2.16	4.42	3.76	6.8
InP	1.34	3.96	4.81	4.5
InAs	0.36	3.59	5.67	1.8
GaSb	0.73	3.53	5.61	2.7
InSb	0.17	2.94	5.78	1.1
GaN	3.39	8.85	6.15	8.9
GaP	2.26	4.94	4.138	6.8

Table 2.
Main properties of the semiconductors considered in this study. From Ref. [8, 10].

number of neutron interactions per unit volume of the material, as discussed in the following. In addition, seven materials (SiC, diamond, GaAs, AlAs, InP, GaN, and GaP) exhibit a bandgap larger than Si and logically, a larger electron-hole pair creation energy (3.6 eV for Si) [10], four materials (Ge, InAs, GaSb, and InSb) are low-bandgap semiconductors (< 1eV) with lower electron-hole pair creation energy than Si. The electrical consequences of this important parameter are discussed in Section 5.

3. Direct evaluation of semiconductor susceptibility to fusion neutrons

The susceptibility of the different semiconductors to neutron irradiation can be firstly evaluated via the calculation of the number of neutron-material interactions under 2.45 or 14 MeV neutrons. This can be performed via a direct analytical calculation using neutron cross-section library data; we considered here the TENDL-2021 nuclear data library [11]. The number of interactions in the target at a fixed neutron energy E is simply given by:

$$N(E) = \sum_i f_i \, \sigma_i(E) \times 10^{-24} \times NV \times e \times M \tag{4}$$

where σ_i is the value at energy E of the cross section for isotope i (in barn), fi is the fraction of isotope i in the target isotopic composition, e is the target thickness, NV is the number of atoms per unit volume, and M is the number of incident monoenergetic neutrons; in this work, fixed to the arbitrary value of 5×10^8 for standardization purpose (introduced in other previous studies [8–10], M initially corresponds to the number of atmospheric neutrons impacting a surface of 1 cm^2 at sea level exposed to natural radiation during 25×10^6 h).

Figure 1 illustrates the extraction from TENDL-2021 library data of the neutron cross-section values at 2.45 and 14 MeV for two different isotopes. Total, elastic, and inelastic data, respectively, correspond to reaction type numbers MT = 1, 2, and 4 in the standardized ENDF format [12]. When it is not available, the cross-section value for the sum of all nonelastic channels (MT = 3) is obtained by subtracting elastic + inelastic cross sections to the total cross section.

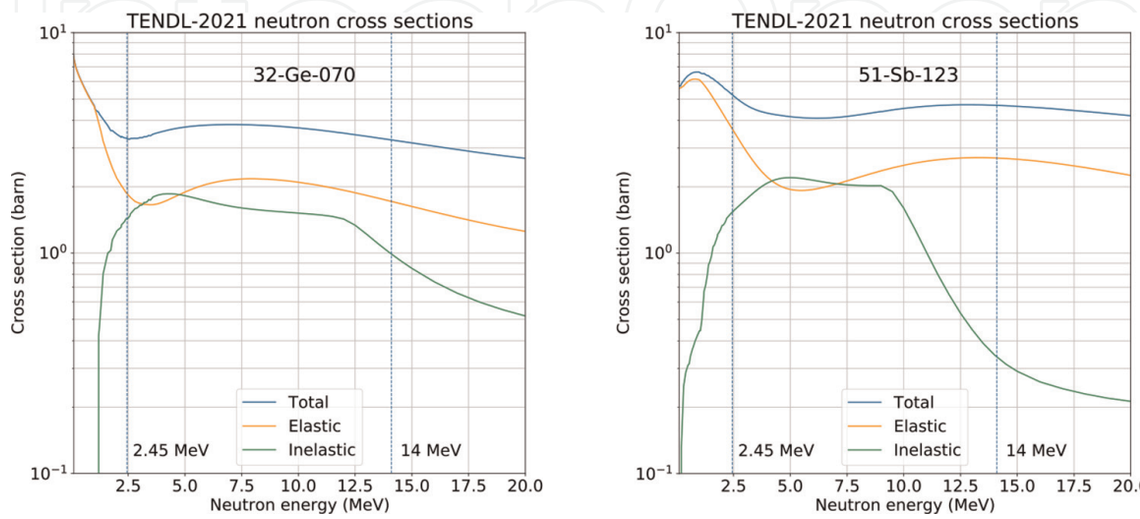


Figure 1.
Example of neutron cross sections (total, elastic and inelastic) extracted from TENDL-2021 nuclear data library [11] for the isotopes 32-Ge-070 (left) and 51-Sb-123 (right).

As the result of this analytical evaluation using Eq. (4), **Table 3** gives the total number of interaction events in a target ($1cm^2 \times 20$ μm) composed of a single chemical element with an isotope distribution corresponding to the natural abundance (**Table 1**) and subjected to 2.45 or 14 MeV neutrons. Values reported in **Table 3** correspond to a normalized value NV = 1.0×10^{22} at/cm^3 for all targets.

From the data of **Table 3**, it is now easy to evaluate the neutron response for any material composed of these elements. **Figure 2** shows the results of this evaluation for the different semiconductor materials, considering their stoichiometry and their exact number of atoms per square centimeter, given in **Table 2**. All numerical values for **Figure 2** are detailed in the Appendix (**Table 6**). From the results of **Figure 2**, we can formulate the following observations:

- Elastic and inelastic interactions dominate for all materials at 2.45 MeV whereas nonelastic interactions represent very roughly one-third of the total number of events at 14 MeV.

- All studied materials exhibit a larger total number of interaction events than silicon, both at 2.45 and 14 MeV.

- Two semiconductors, C (diamond) and GaN show the largest neutron susceptibility at these two energies, followed by SiC.

- Diamond at 2.45 MeV exhibits a pure and extremely high elastic response; this behavior is due to the combination of an important elastic cross section (1.62 barn at 2.45 MeV) and the highest NV value (1.76×10^{23} at/cm^3) between all materials.

- Only a single material, GaN, demonstrates a frank higher response at 14 MeV than at 2.45 MeV in terms of total events (elastic + inelastic + nonelastic),

Target (1.0×10^{22} at/cm^3)	Z	N(E) from Eq.(4) and TENDL-2021					
		2.45 MeV			14 MeV		
		Elastic	Inelastic	Nonelastic	Elastic	Inelastic	Nonelastic
C	6	16,146	0	0	8360	4240	674
N	7	13,201	22	1675	9697	3658	2328
Al	13	25,564	4171	61	7798	4598	5050
Si	14	18,857	6321	0	7555	4922	6706
P	15	28,196	5378	472	7522	2910	8552
Ga	31	16,150	15,009	61	16,839	5908	9892
Ge	32	17,572	16,013	329	17,203	7306	8626
As	33	16,008	17,718	649	17,934	5874	10,119
In	49	31,349	22,255	1735	25,669	4173	16,178
Sb	51	35,376	15,712	612	26,909	3832	15,941

Table 3.
*Total number of interaction events in a target ($1cm^2 \times 20$ μm) composed of a single chemical element with an isotope distribution corresponding to the natural abundance (**Table 1**) and subjected to 2.45 or 14 MeV neutrons. Values are calculated from Eq. (4) with a normalized value NV = 1.0×10^{22} at/cm^3 for all targets.*

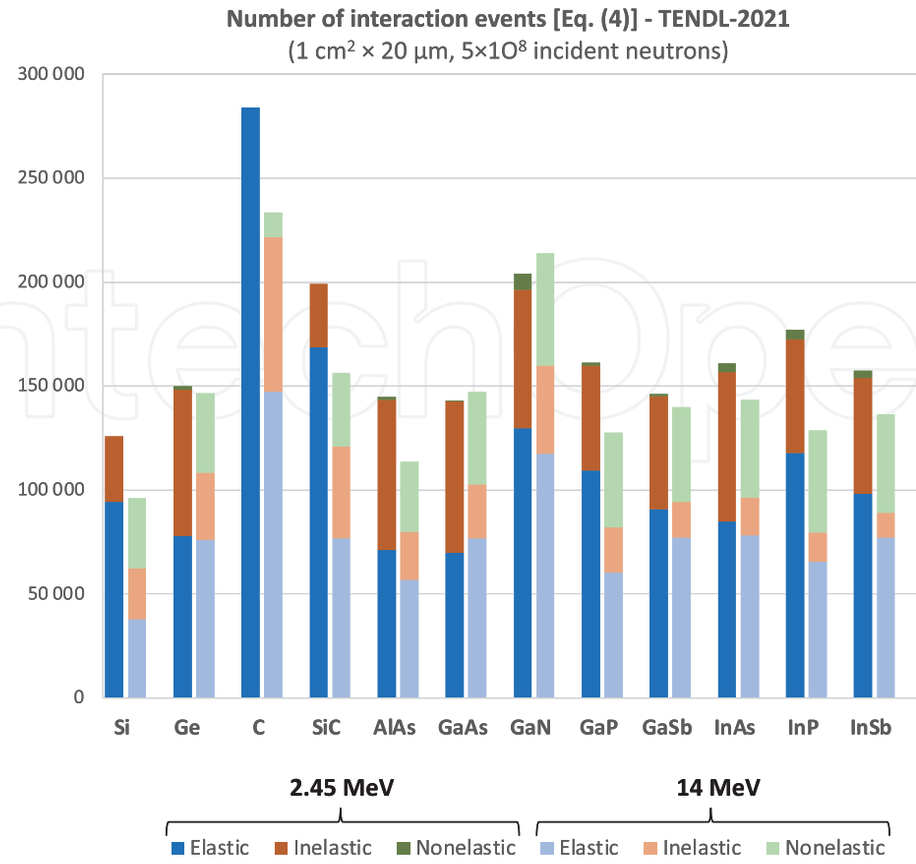


Figure 2.
Number of elastic, inelastic, and nonelastic interaction events in a target ($1cm^2 \times 20\ \mu m$) composed of natural semiconductors and subjected to 5×10^8 neutrons of 2.45 or 14 MeV. Values are deduced from ***Table 3*** *considering the stoichiometry and the exact number of atoms per square centimeter for each material given in* ***Table 2****. Numerical values for this graph are reported in the appendix (****Table 6****).*

due to an elevated number of nonelastic events, the highest at 14 MeV for all materials.

- AlAs exhibits the smallest neutron response after silicon.

All these results are now investigated in detail in the next section via more complete numerical simulations.

4. Geant4 and MCNP6 simulations

4.1 Simulation details

The neutron susceptibility of the studied materials has been in-depth analyzed using the Monte Carlo radiation transport codes Geant4 (version 10.07 patch 02, G4NDL4.6 neutron library [13–15]) and MCNP6 (version 6.2 [16, 17]). In a similar way to previous analytical estimations, natural semiconductor targets ($1\ cm^2 \times 20\ \mu m$) have been subjected to incoming 2.45 or 14 MeV neutrons perpendicularly to their largest surface. The same number of 5×10^8 incident neutrons has been considered for each simulation run.

For Geant4, a simulation run produces a single output file containing all the information related to the neutron interaction events in the target material—nature of

the interaction, spatial coordinates of the reaction vertex, and exhaustive list of secondary particles produced during the interaction (energy and emission direction vector for each of these emitted particles). A post-treatment eliminates all gamma photons, neutral and light particles (e^-, e^+, η), not able to induce significant single-event effects in electronics.

For MCNP6 simulation, PTRAC card options were activated to obtain, for each event, the nature and the coordinates of the vertex of the interaction and the final energy of the neutron after the interaction. It is thus possible to count and to discriminate interactions as a function of the target atom and as a function of their nature (elastic, inelastic, and nonelastic).

4.2 Numbers of interaction events at 2.45 and 14 MeV

Figures 3 and **4** show the number of interaction events for the different semiconductor targets subjected to 2.45 and 14 MeV neutrons, respectively. All the numerical values for these two figures are reported in **Table 6** of the Appendix. These results show a good agreement, on one hand, between analytical and numerical estimations, and, on the other hand, between Geant4 and MCNP6 results. If we consider the total number of interaction events (**Table 6**), analytical and numerical results agree within 6% on average at 2.45 MeV and within 2.4% on average at 14 MeV. Between Geant4 and MCNP6 results, agreements are better, within 3% on average at

2.45 MeV and within 1.6% on average at 14 MeV. The best agreement is obtained for diamond, GaN, and GaAs at 14 MeV, the largest difference is for GaP at 2.45 MeV,

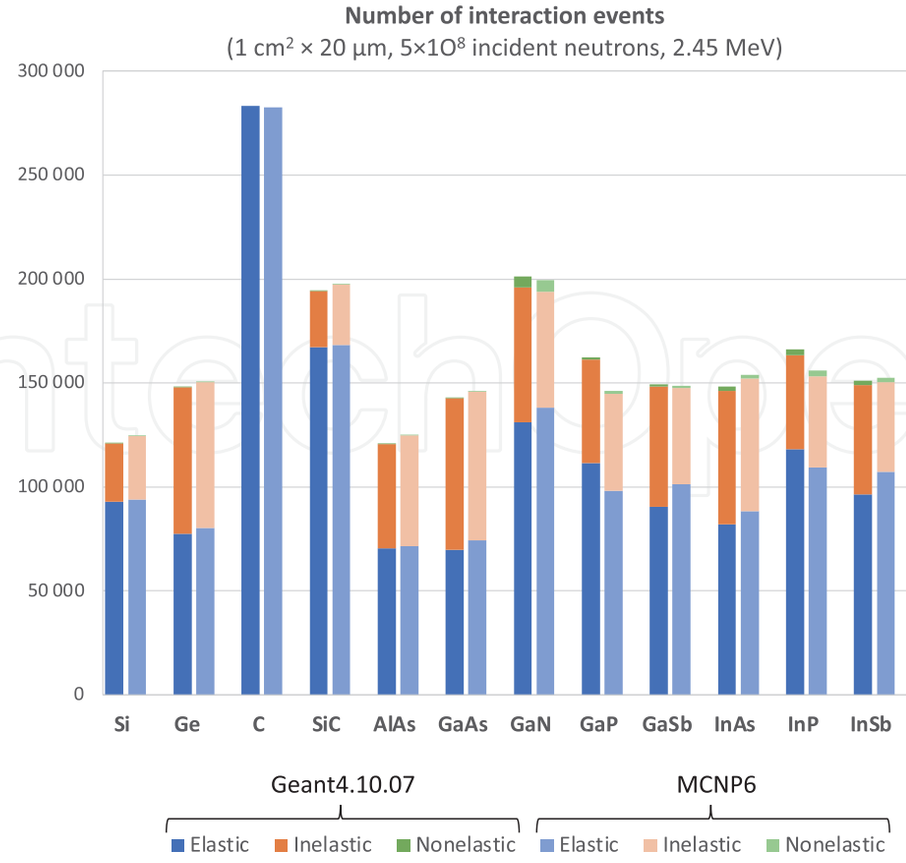


Figure 3.
Number of elastic, inelastic, and nonelastic events estimated by Geant4 and MCNP6 as a function of the nature of the target material for 2.45 MeV incoming neutrons.

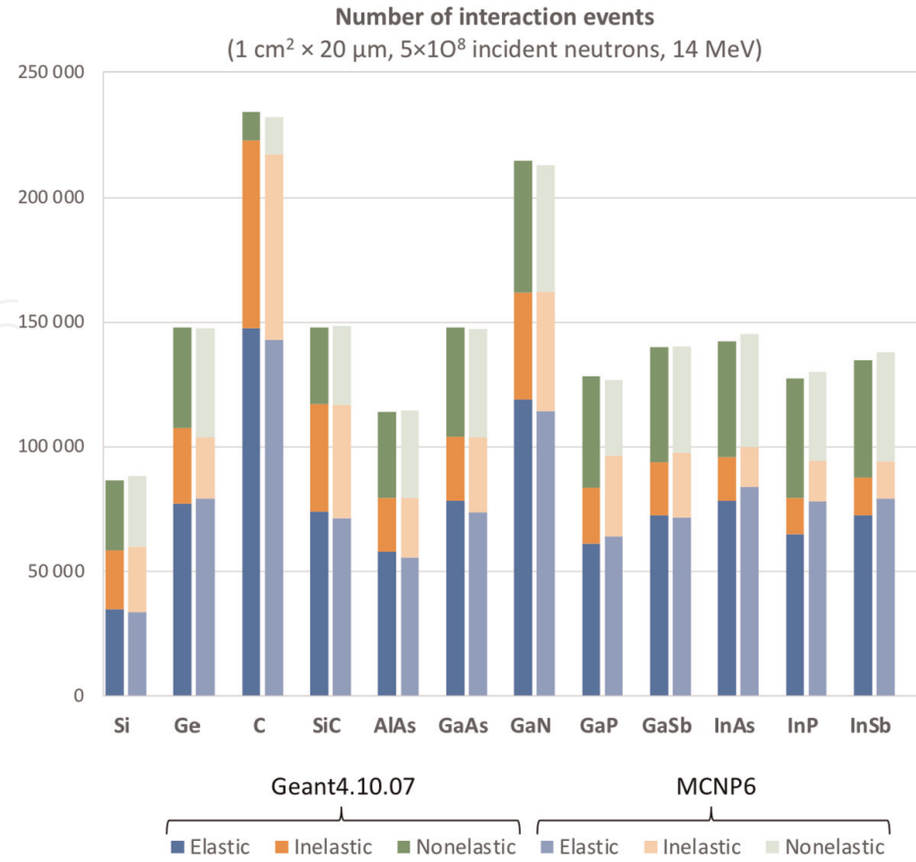


Figure 4.
Number of elastic, inelastic, and nonelastic events estimated by Geant4 and MCNP6 as a function of the nature of the target material for 14 MeV incoming neutrons.

with 11.5% of the variation between Geant4 and MCNP6, the number of elastic events being larger than 14% for Geant4 with respect to MCNP6. Globally, one can see that the different sets of results agree very satisfactorily.

In the following and because Geant4 can track all particles and, consequently, give more exhaustive information about secondaries than MCNP6, we will explore in detail the distributions and characteristics of secondaries produced in the interaction events at both 2.45 and 14 MeV from Geant4 results.

4.3 Detailed analysis at 2.45 MeV

Figures 5–7 shows the energy histograms of the secondaries produced by 2.45 MeV neutrons in the targets composed of the different natural semiconductor materials under investigation. In the particular case of C (diamond), shown in **Figure 5**, all secondaries are exclusively elastic carbon recoil nuclei. They form a continuum from zero to a maximum energy E_{max} theoretically equal to [18]:

$$E_{max} = 4 \times E \times \frac{A}{(A+1)^2} \tag{5}$$

where A is the mass number of the target nucleus and E is the energy of the incident neutrons. Here, for carbon, A = 12 and with E = 2.45 MeV, we obtain a theoretical value of E_{max} = 0.696 MeV, in excellent agreement with the cutoff value of 0.7 MeV extracted from **Figure 5**. This figure also shows a direct comparison between

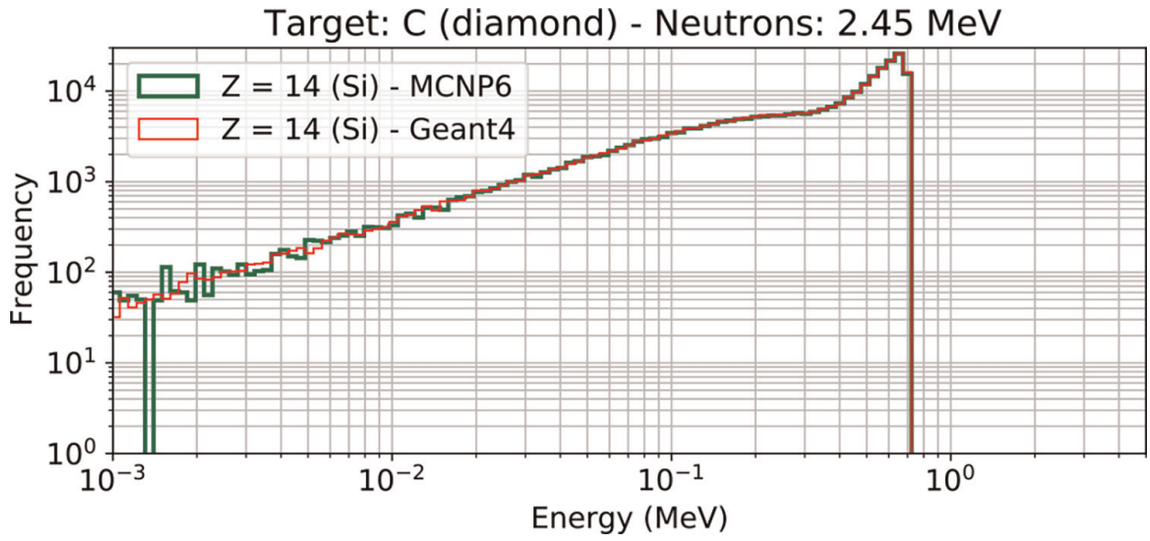


Figure 5.
Energy histograms of secondaries produced in the diamond target by 2.45 MeV neutrons and obtained from Geant4 and MCNP6 simulations. All secondaries are elastic recoil nuclei.

MCNP6 and Geant4 simulation results because, in the case of elastic events, it is possible from MCNP6 output data to compute the energy distribution of recoil nuclei; an estimation unfortunately not possible for inelastic and nonelastic events.

Figures 6 and 7 show Geant4 results for the other target materials. For Si, Ge, SiC, AlAs, GaAs, InAs, InSb, and GaSb (**Figure 6**), 2.45 MeV neutrons produce quasi exclusively, via elastic, inelastic, and nonelastic interactions, secondaries with the same atomic number than one of the elements of the target. The heavier the recoil nucleus or secondary product, the more the distribution is shifted toward the lower energies. This shift is more marked as the difference in atomic number is greater, for example for InP (Z = 15 and 49). Only three materials, i.e., GaN, GaP, and InP, show (**Figure 7**) a significant production of secondaries at 2.45 MeV that differ from target elements:

- For GaP and InP, the presence of phosphorus makes possible the nonelastic reaction $^{31}P(n,p)^{31}Si$ that produces a proton with mean energy around 890 keV. Following this reaction scheme, 980 protons are emitted in GaP and 755 in InP. $^{31}P(n,p)^{31}Si$ represents 88% (resp. 28%) of the nonelastic interactions in GaP (resp. in InP).

- For GaN, the presence of nitrogen makes possible the two nonelastic reactions $^{14}N(n,\alpha)^{11}B$ and $^{14}N(n,p)^{14}C$ that respectively produce an alpha particle (around 1.6 MeV) and a proton (around 2.7 MeV). 4555 alphas and 614 protons are emitted following these two reaction schemas. $^{14}N(n,\alpha)^{11}B$ and $^{14}N(n,p)^{14}C$, respectively, represent 84 and 11% of the nonelastic interactions in GaN.

In addition to the previous analysis, **Figure 8** (left) gives, for each material, the sum of the initial kinetic energy for all produced secondaries (we recall here that neutrons, gamma rays, and light particles, such as electrons or positrons are not considered, only charged particles with $Z \geq 1$ are considered). Such a quantity represents the energy susceptible to be deposited by all these secondaries in the considered target if they are totally stopped (after transferring the totality of their kinetic energy, essentially by ionization process). This energy amount is the highest for C (about 10^5 MeV), followed by SiC, GaN, Si, and GaP (all above 10^4 MeV); it is minimum for InSb (around 3×10^3

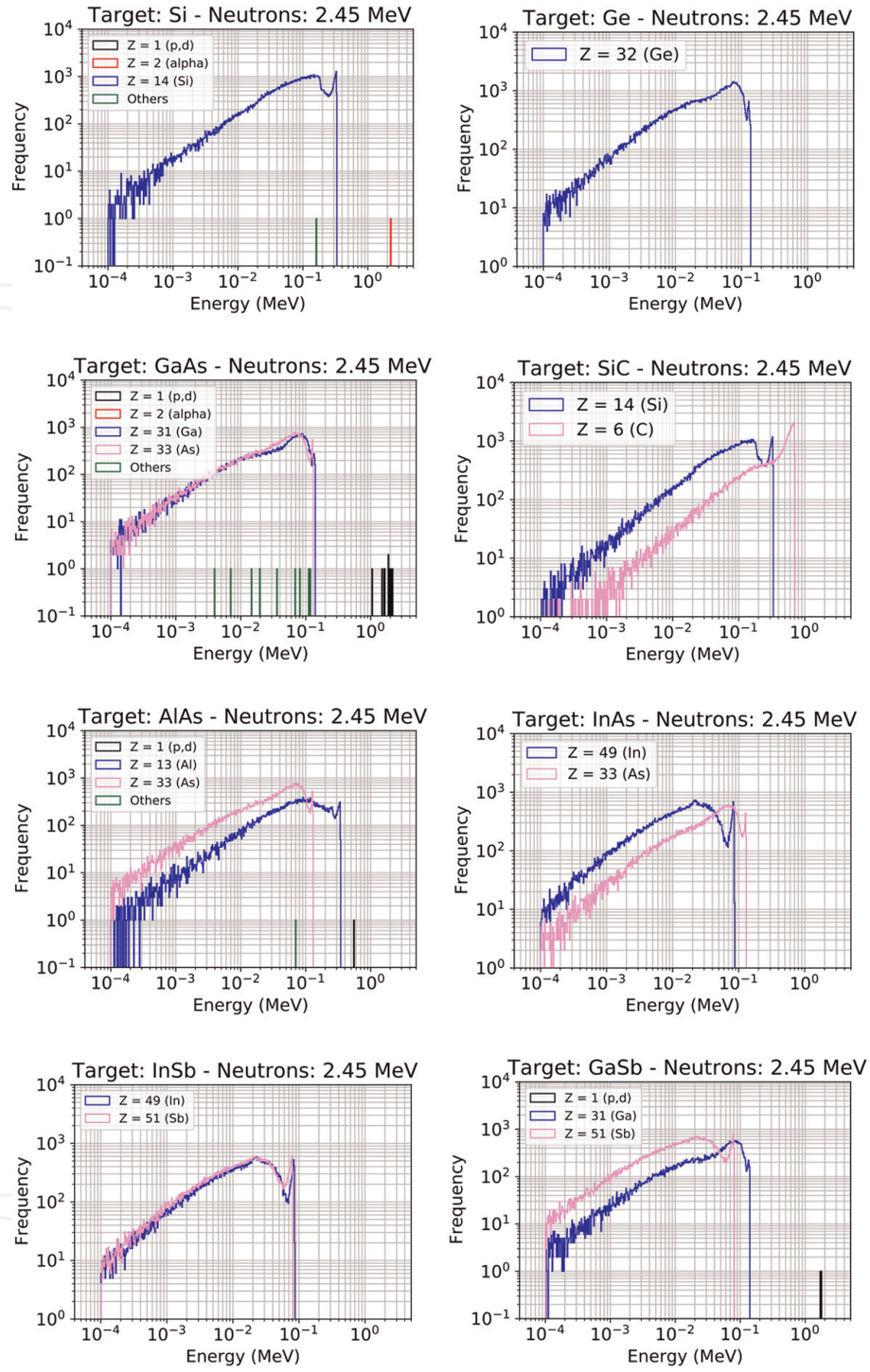


Figure 6.
Energy histograms of secondaries produced by 2.45 MeV neutrons in targets of Si, Ge, GaAs, SiC, AlAs, InAs, InSb, and GaSb semiconductor materials.

MeV). **Figure 8** (right) gives the average energy conveyed per particle for the four categories of secondaries. The consequence of this result on the electrical point-of-view and in the framework of single-event effect occurrence is be discussed in Section 5.

4.4 Detailed analysis at 14 MeV

Figures 9 and **10** show the energy histograms of the secondaries produced by 14 MeV neutrons in the different targets. Contrary to the previous case at 2.45 MeV, a

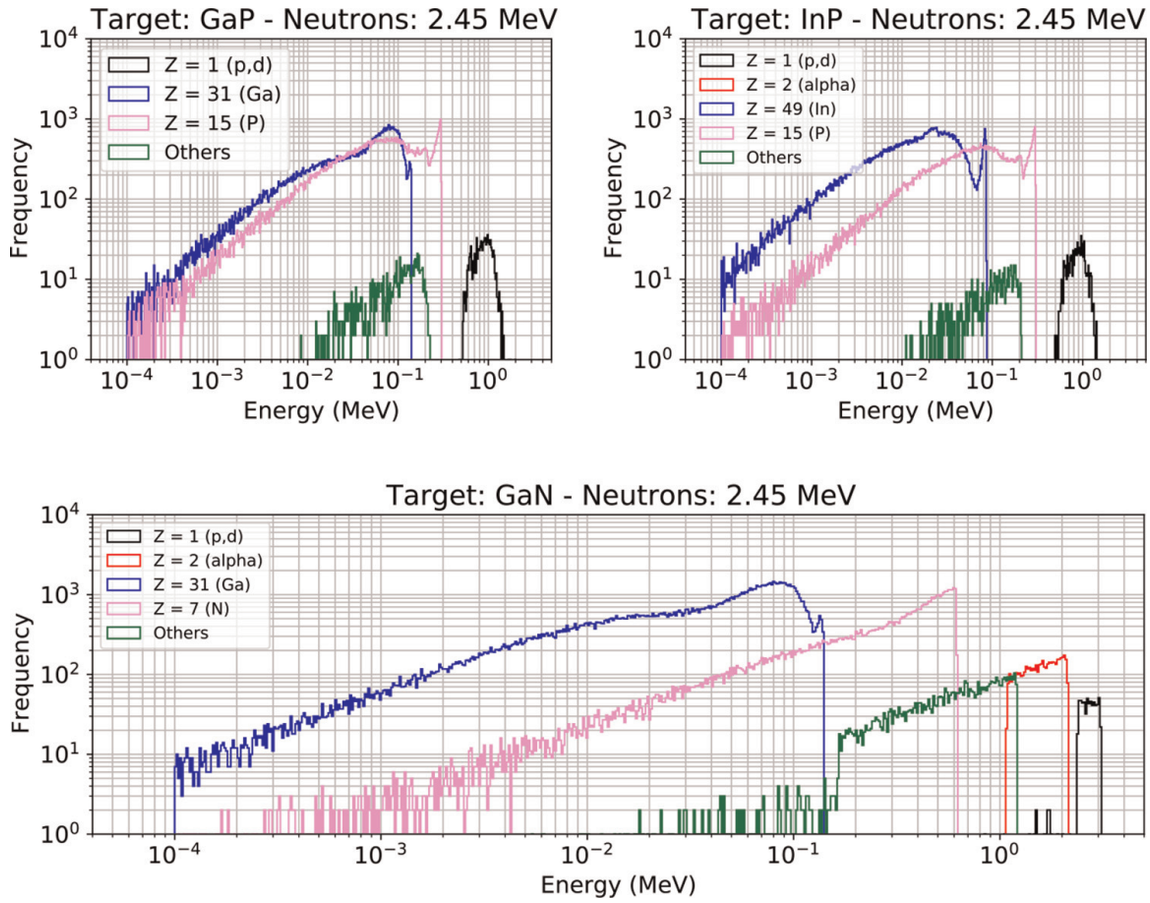


Figure 7.
Energy histograms of secondaries produced by 2.45 MeV neutrons in targets of GaP, InP, and GaN semiconductor materials.

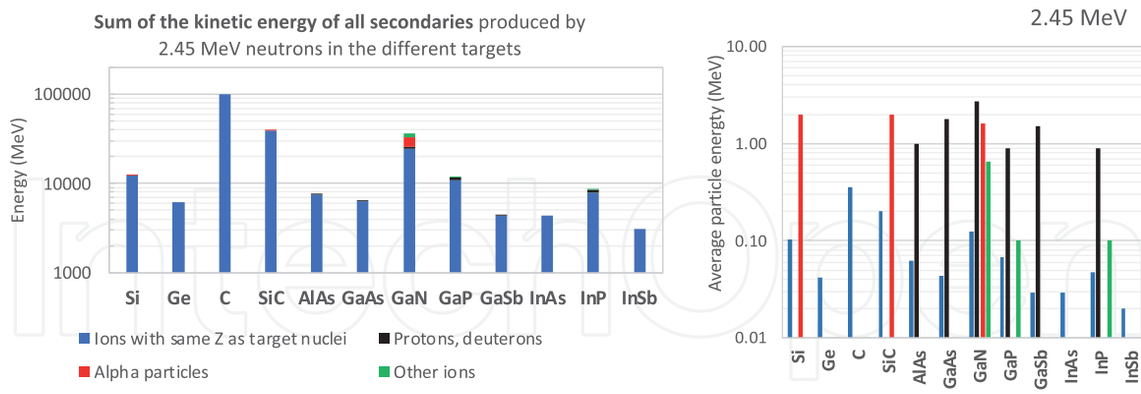


Figure 8.
Left: Sum of the kinetic energy of all secondaries produced by 2.45 MeV in the different targets (charged particle with $Z \geq 1$). Right: Average particle energy per particle type (same legend as for the left figure).

significant number of nonelastic reaction channels is opened at this higher neutron energy. The ratio of the number of nonelastic reactions with respect to the total number of events varies from about 5% in the case of C up to 38% for InP; it is around 33% for Si. These nonelastic reactions produce several types of ions, protons, and alpha particles—their respective numbers are given in **Table 4** which also indicates the number of secondary ions produced characterized by the same atomic number as target nuclei. This last category includes, of course, all recoil nuclei produced in elastic and inelastic reactions but also ions produced in certain nonelastic reactions, for

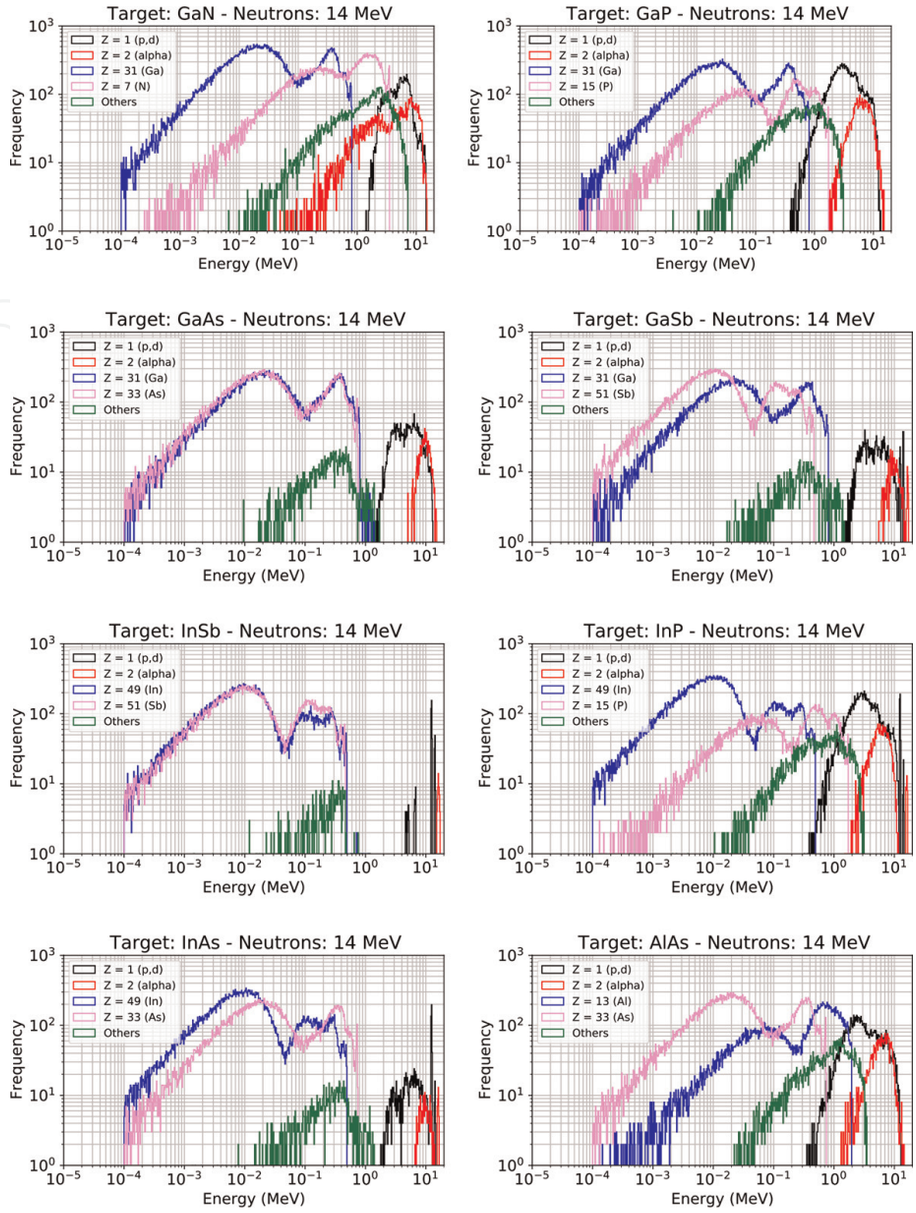


Figure 9.
Energy histograms of secondaries produced by 2.45 MeV neutrons in targets of GaN, GaP, GaAs, GaSb, InSb, InP, InAs, and AlAs III-V semiconductor materials.

example, in the (n,n'γ) or (n,2n'γ) reactions that are increasingly frequent when increasing the atomic number of the target element. These nonelastic reactions give a final nucleus with a lighter mass with respect to the initial impacted nucleus (for example, ^{74}Ge(n,2n)^{73}Ge or ^{115}In(n,2n)^{113}In, etc.).

For the good understanding of **Figures 9** and **10**, **Table 5** indicates the main nonelastic reactions leading to the production of protons and alpha particles. The energy ranges of the ejected particles are also reported. Protons, deuterons, and tritons (Z=1) are produced in large numbers in six materials, by order of importance—GaP, Si, SiC, InP, AlAs, and GaN. The main reactions for these targets are the following (we indicated in parenthesis the energy threshold of the reactions): ^{31}P(n,n'p)^{30}Si (7.5 MeV), ^{31}P(n,p)^{31}Si (0.7 MeV), ^{31}P(n,d)^{30}Si (5.2 MeV), ^{28}Si(n,p)^{28}Al (4 MeV), ^{27}Al(n,p)^{27}Mg (1.9 MeV), ^{14}N(n,d)^{13}C (5.7 MeV). Protons and deuterons are also observed in smaller numbers in the other materials, i.e., GaAs, Ge, GaSb, InAs, and InSb. Only two tritons are observed for C, they are produced in the rare reaction

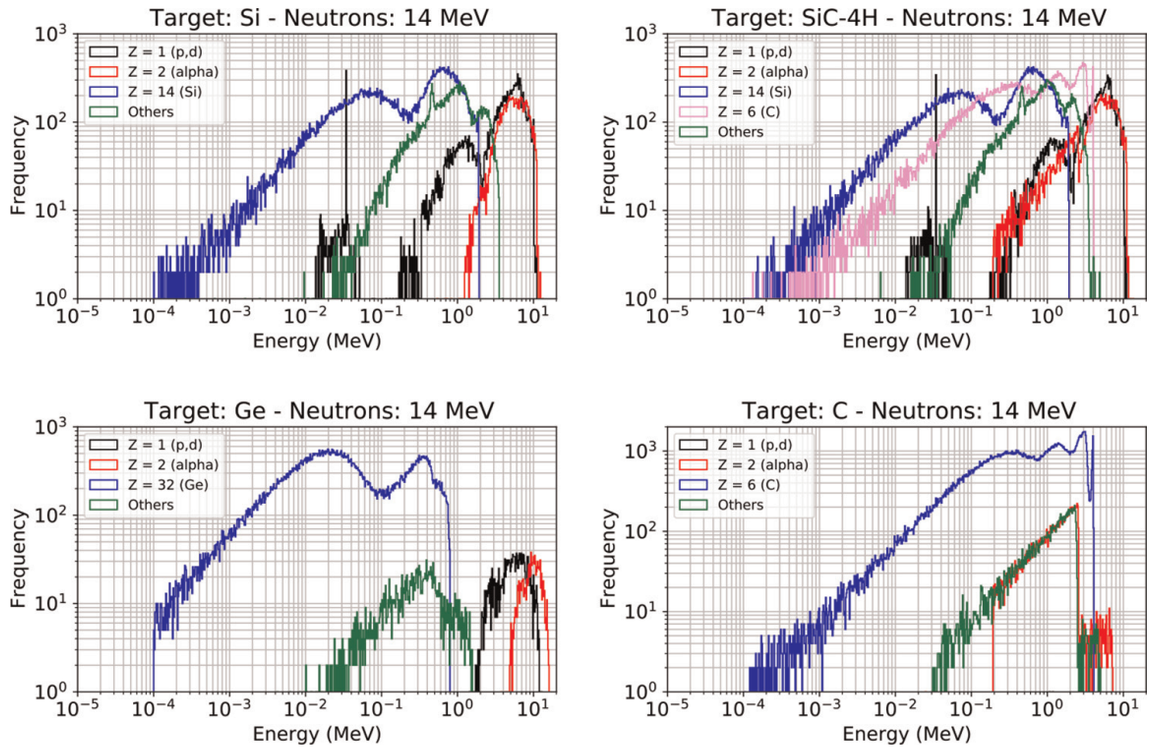


Figure 10.
Energy histograms of secondaries produced by 2.45 MeV neutrons in targets of Si, SiC-4H, Ge, and C (diamond) Group-IV semiconductor materials.

Target	Number of ions with the same Z as target nuclei	Number of protons, deuterons, and tritons	Number of alpha particles	Number of other ions
Si	58,293 (Si)	16,815	10,245	22,968
Ge	107,913 (Ge)	1910	1042	2152
C	222,165 (C)	2	11,460	11,445
SiC	56,611 (Si) + 60,415 (C)	16,376	13,101	25,577
AlAs	26,836 (Al) + 52,924 (As)	10,003	3186	5530
GaAs	51,729 (Ga) + 52,697 (As)	3238	806	1713
GaN	102,776 (Ga) + 59,190 (N)	9377	7295	12,278
GaP	57,127 (Ga) + 26,396 (P)	19,439	4126	7938
GaSb	40,309 (Ga) + 53,776 (Sb)	1874	438	1105
InAs	53,690 (In) + 42,455 (As)	1409	237	1094
InP	58,842 (In) + 20,892 (P)	13,994	2814	5725
InSb	43,067 (In) + 44,737 (Sb)	458	54	484

Table 4.
Number of secondaries produced by 14 MeV neutrons in the different targets.

$^{13}C(n,t)^{11}B$. Concerning alpha particles (Z=2), they are produced in large or significant numbers in seven materials—SiC, C, Si, GaN, GaP, InP, and AlAs. The main reactions for these targets are the following—$^{28}Si(n,\alpha)^{25}Mg$ (2.7 MeV), $^{12}C(n,\alpha)^{9}Be$ (6.2 MeV), $^{14}N(n,\alpha)^{11}B$ (0.17 MeV), $^{31}P(n,\alpha)^{28}Al$ (2 MeV), $^{27}Al(n,\alpha)^{24}Na$ (3.2 MeV). Traces of alpha particles are also observed in Ge, GaAs, GaSb, and InSb.

Element	Main reactions for α, p or d production (14 MeV neutrons)	Energy range of the ejected particle
C	$^{12}C(n,\alpha)^{9}Be$	0.2–7 MeV
N	$^{14}N(n,\alpha)^{11}B$ $^{14}N(n,d)^{13}C$ $^{14}N(n,p)^{14}C$	0.01–14 MeV 0.1–9 MeV 5–12 MeV
Al	$^{27}Al(n,\alpha)^{24}Na$ $^{27}Al(n,p)^{27}Mg$	1.8–14 MeV 0.4–13 MeV
Si	$^{28}Si(n,d)^{27}Al$ $^{28}Si(n,p)^{28}Al$ $^{28}Si(n,\alpha)^{25}Mg$	10–50 keV (peak at 34 keV) 2–10 MeV 0.5–13 MeV
P	$^{31}P(n,\alpha)^{28}Al$ $^{31}P(n,n'p)^{30}Si$	0.2–12 MeV 0.4–11 MeV
Ga	$^{69}Ga(n,\alpha)^{66}Cu$ $^{69}Ga(n,p)^{69}Zn$	4–14 MeV 0.01–14 MeV
Ge	$^{70}Ge(n,\alpha)^{67}Zn$ $^{70}Ge(n,p)^{70}Ga$	4–14 MeV 1.5–13 MeV
As	$^{75}As(n,\alpha)^{72}Ga$ $^{75}As(n,p)^{75}Ge$	4–14 MeV 1–13 MeV
In	$^{115}In(n,p)^{115}Cd$	10–14 MeV
Sb	$^{123}Sb(n,p)^{123}Sn$	12–14 MeV

Table 5.
*Main reactions for proton, deuteron, or alpha particle production in the nonelastic interactions of 14 MeV neutrons with target elements. The energy ranges of the ejected particles are also indicated (see **Figures 9** and **10** for visualization).*

Figure 11 (left) shows the sum of the kinetic energy of all secondaries produced by 14 MeV in the different targets. **Figure 11** (right) gives the average energy conveyed per particle for the four categories of secondaries. Protons and alphas are of prime importance in the radiation response of these materials insofar as they convey a very important part of the total kinetic energy; this part is predominant in the case of five materials—Si, SiC, AlAs, GaN, and GaP. As compared to **Figure 8** (left) obtained for 2.45 MeV neutrons, the amplification factor of the total kinetic energy at 14 MeV for

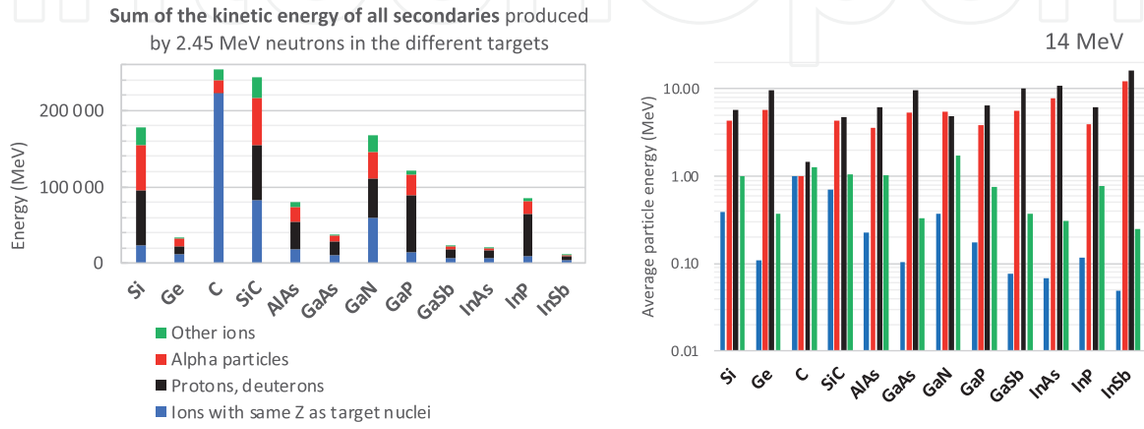


Figure 11.
Left: Sum of the kinetic energy of all secondaries produced by 14 MeV in the different targets (charged particle with $Z \geq 1$). Right: Average particle energy per particle type (same legend as for the left figure).

all secondaries is minimal for C (×2.5) and InSb ((×3.5) and maximal for InP, GaP, AlAs (around ×10), and Si (×14.3).

5. Implication for electronics subjected to fusion neutrons

In this last section, we examine the previous results in light of the mechanisms of creation of single-event effects (SEEs) in electronics subjected to fusion neutrons. We recall here that these SEEs are initiated by neutron-matter interactions in four main steps—(1) interactions produce secondary fragments or recoil nuclei from target nuclei. (2) The produced ion(s) interact(s) with material to generate free charge carriers via the production of electron and hole pairs. (3) Electrons and holes are transported by drift-diffusion mechanisms through the circuit materials (oxides and semiconductors) up to a sensitive node (reversely biased junctions); free carriers also recombine during their transport. (4) The collected charge on a sensitive node can significantly alter its voltage that leads to a change in device or circuit operation. This voltage glitch may propagate through the circuit. The present work allows us to provide quantitative information on steps 1 and 2 in so far as from step 3, it would be necessary to consider the circuit architecture, the applied polarizations, and the transport and recombination properties of the materials. In the following, we examine the different materials in light of the number of interactions and of the number of e-h pairs created on average per interaction.

Concerning the first metric, the number of SEEs susceptible to be created in an electronic circuit (of the same geometry as the target for simplicity) is at most equal to the number of interaction events that can deposit enough energy, i.e., create a sufficient electrical charge able to disturb the circuit operation (in the case of an SRAM memory, this minimum amount of charge susceptible to upset a memory cell is called a critical charge). This number of SEEs is not easy to evaluate but it can be upper bounded by the number of events that can deposit energy and therefore generate an electrical charge greater than or equal to the critical charge of the circuit. To roughly estimate this metric from the histogram of the energies/charges deposited per event, a simple transformation is necessary, as illustrated in **Figure 12**. **Figure 12** (left) shows the energy histograms (frequency and cumulative frequency histograms) for all the events produced by 2.45 MeV and 14 MeV neutrons in GaP. The relationship between energy (bottom scale) and charge (top scale) considers the energy value of the creation of electron-hole pairs, as given in **Table 2**.

At fixed energy or charge, the cumulative frequency histogram directly indicates the number of events for which the total energy deposited is below this value. In practice, it is more convenient to have the complementary value, i.e., the number of events above this value is plotted in **Figure 12** (right), and directly expressed in electrical charge instead of energy. Applying this transformation to all targets gives the ensemble of cumulative histograms, as shown in **Figures 13** and **14**.

These figures can be directly used to estimate the number of events able to deposit an electrical charge superior to a given value. From this data and knowing a minimum of geometric and electrical characteristics of the circuit to be evaluated from a radiative point of view (number and geometry of the sensitive volumes, critical charge, etc.), it would be possible, in future studies, to estimate the number of events susceptible to produce SEEs at both 2.45 and 14 MeV.

Figures 13 and **14** provide also other interesting information about the difference in the neutron susceptibility of a given material at these two energies—the greater this

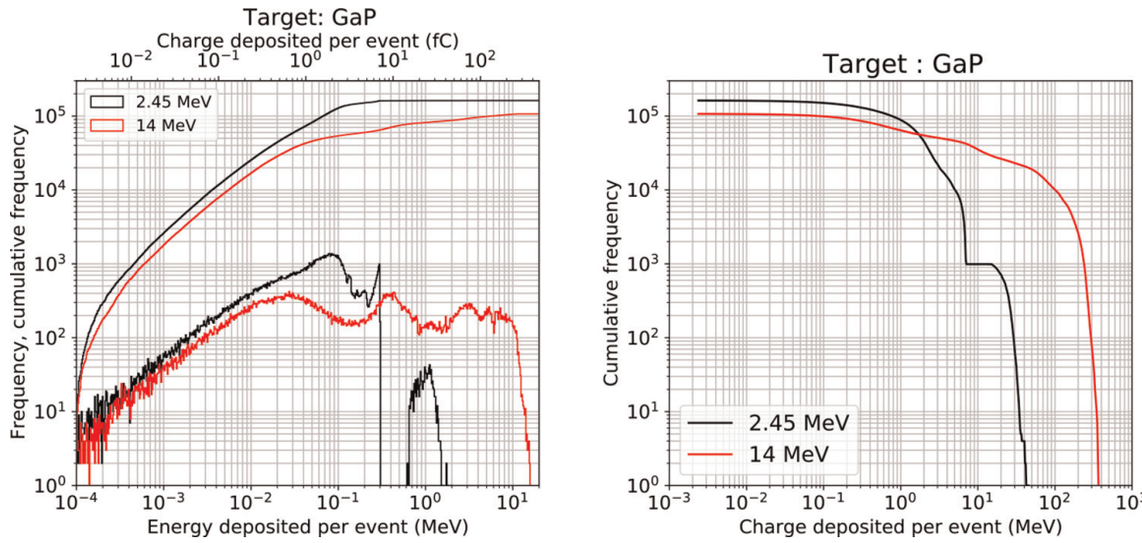


Figure 12.
Left: Histogram and cumulative histogram of the energy deposited per event for all interaction events in GaP target. Right: Reversed cumulative histogram from the left figure expressed in charge deposited per event (MeV).

difference, the more the material, and therefore, the circuit based on this semiconductor will be likely to present a significant difference in its radiative SEE response. This difference can be appreciated following two criteria—the respective amounts of events at the lowest charge deposited per event (here at 10^{-2} fC) and the "distance" between the shoulders of the curves at the highest charge values. For example, a circuit based on diamond or GaN semiconductor may logically presents less difference between its SEE responses at 2.45 MeV and 14 MeV than a circuit based on germanium, InSb, or InAs. Of course, this difference in neutron sensitivity is also dependent on the critical charge value of the considered circuit. In the case of GaAs, for example, a circuit with a 10 fC of critical charge should be quasi-immune to

2.45 MeV neutrons but sensitive to 14 MeV. To go further in this analysis and be quantitative, it would be of course necessary to consider the cumulative histograms of the charge collected at each event. The passage from the deposited charge to the collected charge requires numerical simulations on a given architecture and modeling of transport, recombination, and collection mechanisms, a work currently in progress.

Concerning the second metric, **Figure 15** gives the number of e-h pairs created in average per interaction for the different targets at the two neutron energies. At 2.45 MeV, this value is minimum for AlAs (78,000) and maximum for diamond (29,000) and Si (27,000). The average level and the relative low dispersion of these values indicate that recoil nuclei, very widely produced in these elastic and inelastic reactions, deposit small amounts of charges over very short distances of a few nanometers to a few hundred nanometers (data not shown). At 14 MeV, the results of **Figure 15** (right) show higher values (approximately $\times 3$ to $\times$ 12 for the different materials, and $\times$ 20 for Si) due to the contributions of nonelastic reactions that produce the most energetic secondaries, notably protons and alpha particles. Surprisingly and contrary to the case of irradiation with atmospheric neutrons [10], Silicon sensibly differs from the other materials at 14 MeV since it has the greatest multiplying factor between

2.45 and 14 MeV. This is due to a relatively low number of events (86 kilo events) at this energy with respect to the other semiconductors (**Table 6**) combined with an important level of production of protons and alpha particles (**Table 3**) and also with an energy value of e-h pair creation inferior to the average value (around 5 eV) for all

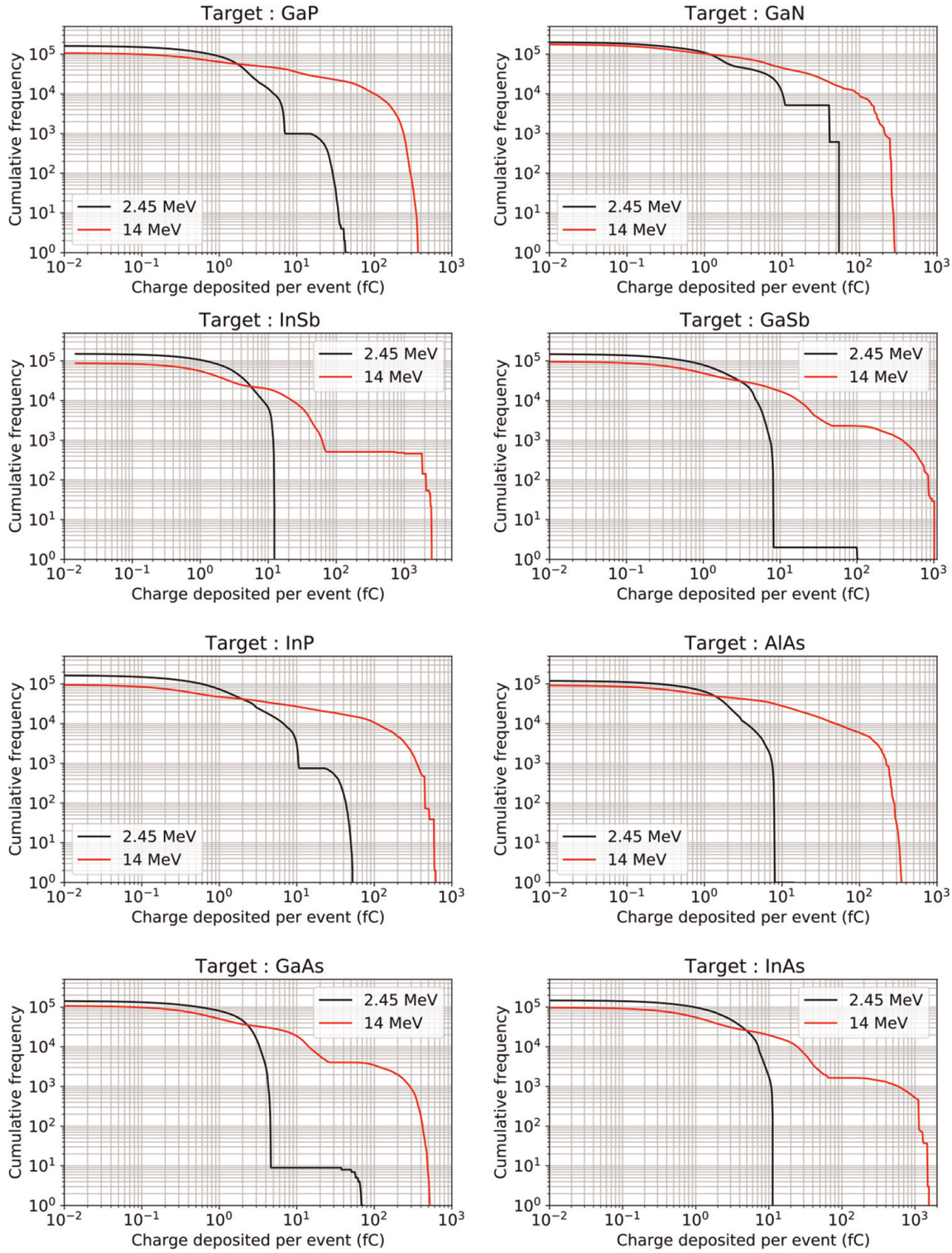


Figure 13.
Reversed cumulative histogram of the energy deposited per event for all interaction events in GaP, GaN, InSb, GaSb, InP, AlAs, GaAs, and InAs targets subjected to 2.45 MeV and 14 MeV neutrons. For a fixed value of the deposited charge, the curves give the number of interactions able to deposit at most this energy in the corresponding target.

materials (**Table 2**). The other materials which exhibit high values are SiC, GaP, and InP. Statistically, in these four materials, a neutron-target interaction at 14 MeV will deposit more charge than in the other materials, which potentially makes these events more threatening for the creation of SEEs. The balance between all these factors is, therefore, not obvious when one remains at the only "material" level for these studies.

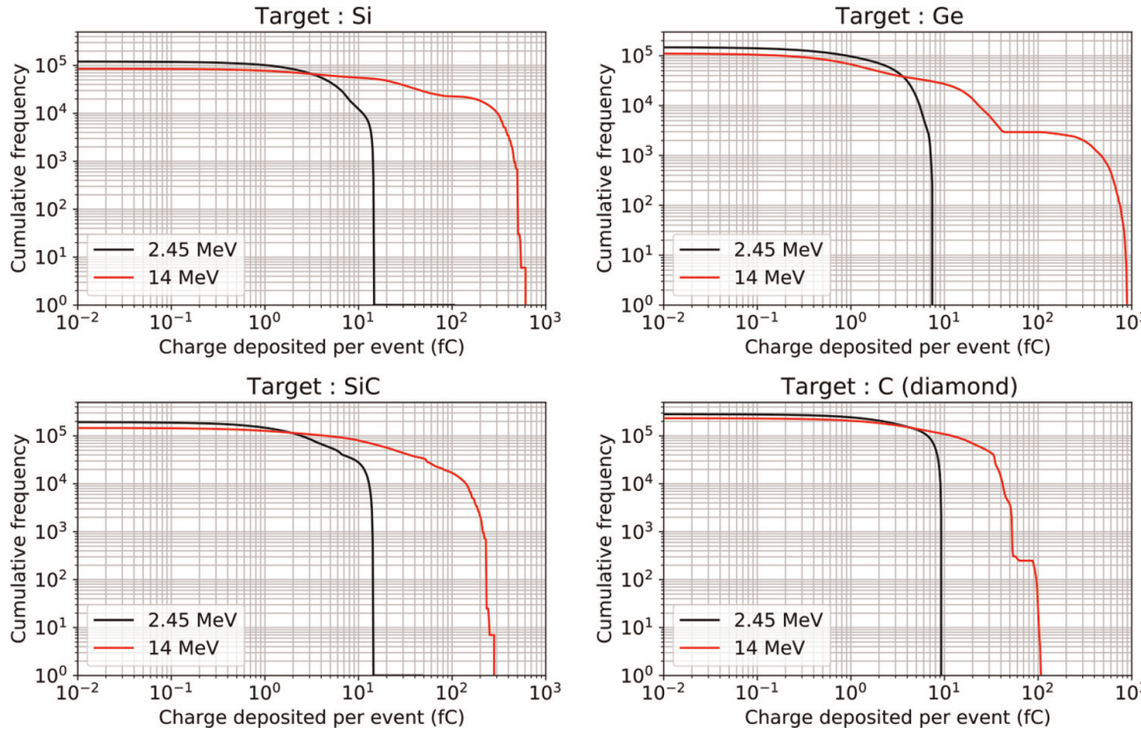


Figure 14.
Reversed cumulative histogram of the energy deposited per event for all interaction events in Si, Ge, SiC, and C (diamond) targets subjected to 2.45 MeV and 14 meV neutrons. For a fixed value of the deposited charge, the curves give the number of interactions able to deposit at most this energy in the corresponding target.

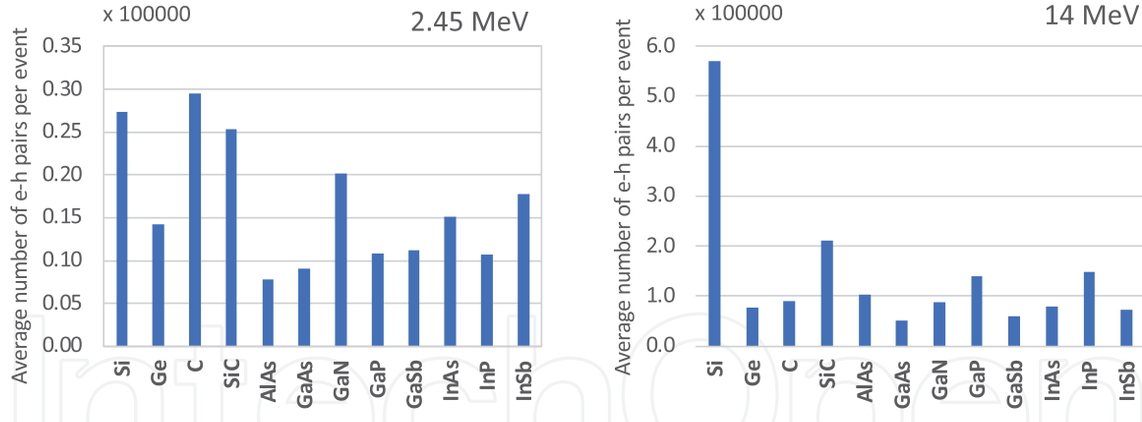


Figure 15.
The average number of e-h pairs created per interaction event in the different targets subjected to 2.45 MeV (left) and 14 MeV (right) neutrons.

This point requires numerical simulations at the circuit level to go further in the investigation of the level of SEE in electronics based on these different materials.

6. Conclusion

This work explored the radiation response of Group IV (Si, Ge, SiC, diamond) and III-V (GaAs, GaN, GaP, GaSb, InAs, InP, InSb, AlAs) semiconductors subjected to D–D (2.45 MeV) and D–T (14 MeV) neutrons. This first study was limited to the level of the neutron response of bulk materials, an essential step to be able, subsequently, to study the response of electronic components and circuits based on these materials. The response of each semiconductor has been systematically investigated through a

direct calculation using nuclear cross-section libraries, MCNP6, and Geant4 numerical simulations. The counting of reaction rates per type of reaction (elastic, inelastic, nonelastic), as well as the classification of all neutron-induced secondary products as a function of their nature and energy, gives a first very complete picture of the behavior of these materials in a fusion environment under D–D or D–T neutrons. Although all studied materials exhibit a larger total number of interaction events than silicon, both at 2.45 and 14 MeV, there is nothing to conclude at this stage that they will present a larger response in terms of SEEs at circuit level since this higher neutron susceptibility only relates to the overall number of events and not to the production of the most energetic particles, such as protons or alpha particles. Moreover, such a higher neutron response may be compensated by other mechanisms at the electronics level, for example, a higher energy value of e-h pair creation (which has the effect of reducing the charge deposited) or higher carrier mobility (which can increase the performance of transistors and strengthen the resilience of circuits to single events). Future studies at the circuit level, following a methodology similar to a first study carried out on GaN subjected to atmospheric neutrons [19], will be largely based on the interaction event databases compiled during this first work and will provide more quantitative information to precisely assess the D–D and D–T neutron radiation response of future circuits based on these alternative materials to the classical silicon of microelectronics.

Conflict of interest

The authors declare no conflict of interest.

Appendix

Target (natural material)	Library or simulation code	Number of interaction events ($1cm^2 \times 20$ µm, 5×10^8 neutrons)					
		2.45 MeV			14 MeV		
		Elastic	Inelastic	Nonelastic	Elastic	Inelastic	Nonelastic
Si	TENDL-2021	94,285	31,604	0	37,776	24,611	33,529
	Geant4.10.07	92,927	27,897	4	34,665	23,623	28,341
	MCNP6.2	94,098	30,426	22	33,452	26,309	28,547
Ge	TENDL-2021	77,667	70,778	1456	76,038	32,294	38,127
	Geant4.10.07	77,565	70,315	305	77,241	30,662	40,281
	MCNP6.2	80,378	70,084	323	79,224	24,639	43,772
C	TENDL-2021	284,170	0	0	147,136	74,624	11,862
	Geant4.10.07	283,451	0	0	146,732	75,433	11,462
	MCNP6.2	282,482	0	0	142,767	74,664	14,726
SiC-4H	TENDL-2021	168,715	30,466	0	76,711	44,162	35,570
	Geant4.10.07	167,221	26,879	7	73,700	43,317	30,745
	MCNP6.2	168,151	29,333	20	71,230	45,704	31,559
AlAs	TENDL-2021	71,069	72,328	1570	56,868	23,143	33,523
	Geant4.10.07	70,519	50,256	208	57,846	21,907	34,300
	MCNP6.2	71,557	53,096	194	55,500	23,968	35,153

Target (natural material)	Library or simulation code	Number of interaction events ($1cm^2 \times 20$ µm, 5×10^8 neutrons)					
		2.45 MeV			14 MeV		
		Elastic	Inelastic	Nonelastic	Elastic	Inelastic	Nonelastic
GaAs	TENDL-2021	69,858	72,905	334	76,848	26,038	44,225
	Geant4.10.07	69,858	72,905	334	78,127	26,069	43,719
	MCNP6.2	74,428	71,515	354	73,757	30,081	43,452
GaN	TENDL-2021	129,877	66,514	7683	117,421	42,330	54,074
	Geant4.10.07	130,978	65,011	5420	119,180	42,761	52,815
	MCNP6.2	138,249	55,632	5573	114,349	47,939	50,588
GaP	TENDL-2021	109,534	50,357	1317	60,171	21,781	45,557
	Geant4.10.07	111,630	49,735	1111	60,853	22,646	44,911
	MCNP6.2	98,073	46,664	1309	64,006	32,412	30,478
GaSb	TENDL-2021	90,943	54,223	1189	77,215	17,192	45,596
	Geant4.10.07	90,310	57,992	1072	72,605	21,477	46,037
	MCNP6.2	101,262	46,366	1026	71,519	26,181	42,512
InAs	TENDL-2021	85,006	71,752	4280	78,268	18,035	47,203
	Geant4.10.07	82,040	64,307	2007	78,346	17,799	46,801
	MCNP6.2	88,362	63,776	1824	83,978	15,828	45,441
InP	TENDL-2021	117,899	54,714	4370	65,719	14,025	48,965
	Geant4.10.07	118,171	45,215	2689	65,177	14,538	48,000
	MCNP6.2	109,501	43,783	2720	77,879	16,575	35,607
InSb	TENDL-2021	98,085	55,811	3451	77,290	11,768	47,215
	Geant4.10.07	96,303	52,707	2264	72,622	15,152	47,707
	MCNP6.2	107,126	43,471	2080	79,225	14,813	43,781

Table 6.
*Details of numerical values for **Figures 2–4**.*

Author details

Jean-Luc Autran* and Daniela Munteanu
Aix-Marseille University, CNRS, University of Toulon, Faculté des Sciences, Marseille Cedex, France

*Address all correspondence to: daniela.munteanu@univ-amu.fr

IntechOpen

© 2022 The Author(s). Licensee IntechOpen. This chapter is distributed under the terms of the Creative Commons Attribution License (http://creativecommons.org/licenses/by/3.0), which permits unrestricted use, distribution, and reproduction in any medium, provided the original work is properly cited. CC BY

References

[1] ITER. Unlimited Energy [online]. Available from: http://www.iter.org

[2] Lee S. Advanced Material and Device Applications with Germanium. London: IntechOpen; 2017

[3] Kimoto T, Cooper JA. Fundamentals of Silicon Carbide Technology: Growth, Characterization, Devices, and Applications. Singapore: John Wiley & Sons; 2014

[4] Oktyabrsky S, Ye P. Fundamentals of III-V Semiconductor MOSFETs. Berlin: Springer Science & Business Media; 2010

[5] Li T, Mastro M, Dadgar A. III–V Compound Semiconductors: Integration with Silicon-Based Microelectronics. Boca Raton: CRC Press; 2016

[6] Wesson J. Tokamaks. 4th ed. Oxford: Oxford Science Publication; 2011

[7] Morse E. Nuclear Fusion. Cham: Springer Nature Switzerland AG; 2018

[8] Munteanu D, Autran JL. Susceptibility of group-IV and III-V semiconductor-based electronics to atmospheric neutrons explored by geant4 numerical simulations. In: Rao SP, editor. Numerical Simulations in Engineering and Science. London: IntechOpen; 2017

[9] Munteanu D, Autran JL. Interactions between Terrestrial Cosmic-Ray Neutrons and III-V Compound Semiconductors. In: Valdman J, Marcinkowski L, editors. Modeling and Simulation in Engineering – Selected Problems, Edited by. London: IntechOpen; 2020

[10] Autran JL, Munteanu D. Atmospheric neutron radiation response of III-V binary compound semiconductors. IEEE Transactions on Nuclear Science. 2020;**67**:1428-1435

[11] TENDL-2021. TALYS-Based Evaluated Nuclear Data Library [online]. Available from: https://tendl.web.psi.ch/tendl_2021/tendl2021.html

[12] ENDF Manual. Appendix B: Definition of Reaction Types [online]. Available from: https://www.oecd-nea.org/dbdata/data/manual-endf/endf102_MT.pdf

[13] Agostinelli S et al. Geant4 – A simulation toolkit. Nuclear Instruments and Methods in Physics Research Section A: Accelerators, Spectrometers, Detectors and Associated Equipment. 2003;**506**(3):250-303

[14] Allison J, Amako K, Apostolakis J, Arce P, Asai M, et al. Recent developments in Geant4. Nuclear Instruments and Methods in Physics Research Section A: Accelerators, Spectrometers, Detectors and Associated Equipment. 2016;**835**:186-225

[15] Geant4, Geant4 10.7 Release Notes [online]. Available from: https://geant4-data.web.cern.ch/ReleaseNotes/ReleaseNotes4.10.7.html

[16] Werner CJ et al. MCNP6.2 release notes. Los Alamos National Laboratory, report LA-UR 18-20808. 2018

[17] C.J. Werner (editor), MCNP User's Manual – Code Version 6.2, Los Alamos National Laboratory, report LA-UR 17-29981, 2017

[18] Autran JL, Munteanu D. Soft Errors: From Particles to Circuits. Boca Raton (FL), USA: Taylor & Francis/CRC Press; 2015

[19] Munteanu D, Autran JL. Terrestrial neutron-induced single events in GaN. Microelectronics Reliability. 2019;**100**: 113357